ISSN 1063-7745, Crystallography Reports, 2012, Vol. 57, No. 5, pp. 676–681. © Pleiades Publishing, Inc., 2012.
Original Russian Text © V.G. Kohn, M.A. Orlov, 2012, published in Kristallografiya, 2012, Vol. 57, No. 5, pp. 756–761.

On the 100th anniversary of the discovery of X-ray diffraction

Computer Analysis of Two-Dimensional Images in the Zernike Phase Contrast Method for Hard X Rays

V. G. Kohn[a] and M. A. Orlov[b]

[a] *National Research Centre "Kurchatov Institute," pl. Akademika Kurchatova 1, Moscow, 123182 Russia*
e-mail: kohnvict@yandex.ru
[b] *Moscow State University, Moscow, 119991 Russia*

Received March 25, 2012

Abstract—The problems of the numerical simulation of two-dimensional images in the Zernike phase contrast method in hard X rays are analyzed. Calculations are performed for experimental conditions typical of third-generation synchrotron radiation sources (ESRF, APS, Spring-8, etc.). Schemes are considered where the focusing elements are a refracting lens and a zone plate and the phase-shifting element is situated at the point of the source image. It is shown that the refracting lens allows better resolution than the zone plate. A technique similar to ptychography can be successfully applied to improve the quality of the images obtained by the Zernike phase contrast method.

DOI: 10.1134/S1063774512050082

INTRODUCTION

With the advent of third-generation synchrotron sources (ESRF, APS, Spring-8, etc.), where X-ray beams have a high degree of spatial coherence, the phase contrast method [1], which allows a nondestructive study of the internal structure of weakly absorbing noncrystalline objects, became widespread. In this method, the change in the phase (rather than amplitude) of the wave passing through an object is registered; the data obtained allow one to learn information about the object. However, this method has some shortcomings. First, it yields not the direct image of an object but only the Gabor hologram from which the object should be reconstructed. In fact, this hologram reproduces the contours of the object only at small distances (in the near field). In the Fraunhofer diffraction region, the hologram is essentially different from the object image. Reconstruction is not a simple problem, because the change in the field amplitude related to the change in the phase during radiation propagation in air is registered, while the beam coherence is incomplete and the solution of an inverse problem by the known methods of deriving a phase from two intensities can yield unpredictable distortions.

Second, this method is weakly sensitive to smooth variations of density in an object. Third, it was shown in [2] that this method is ineffective in the study of submicron objects. The above shortcomings can be avoided by the use of the Zernike phase contrast method [3], which is widely employed in optics, in the X-ray range. Lately, the Zernike method has been used only in a few experimental studies, e.g., in [4–6], where the focusing element was a zone plate. In [7], the experiment on the visualization of microobjects involving the Zernike method in the one-dimensional case was numerically simulated. It was shown that a refracting lens used as an objective allows a better resolution.

This study is the second part of the investigation started in [7]. Below we present the results of two-dimensional calculations, which confirm and supplement the results of [7]. We also show that the image quality can be significantly improved using a method similar to ptychography [8], where a diaphragm is inserted into the object plane and the object image is obtained by parts.

SCHEMATIC OF NUMERICAL EXPERIMENT AND CALCULATION METHOD

A schematic of the experiment is shown in Fig. 1. Let r_1, r_2, r_3, and r_4 be the distances from the X-ray source to the object, the focusing element (a lens or a zone plate), the point of source focusing, and the coordinate detector. An object O is situated at the double focal distance from the focusing element (object L); i.e., $r_2 - r_1 = 2F$. A phase-shifting element (object S) is placed at the source image point ($r_3 = r_2 + F/(1 - F/r_2)$, which was determined from the lens formula (here, F is the focal distance of the lens). A detector (object D) is placed at the distance $r_4 - r_2 = 2F$ from the lens. As a result, the image is inverted and not enlarged.

When solving the problems of hard-X-ray propagation, the paraxial approximation is satisfied with high accuracy. Correspondingly, the X-ray transport in air is described by the Kirchhoff integral formula for the solution to the Maxwell equations. Let the z axis of the Cartesian coordinate system be parallel to the optical axis along which the radiation propagates. The problem consists of a calculation of the dependence of the wave field amplitude on the transverse coordinates x and y at each point on the z axis. The specific feature of this problem is the fact that the wave field changes significantly in the transverse directions at distances less than a micron, while the characteristic range of the wave field variation along the z axis exceeds 1 cm. Since the polarization does not change in the processes under consideration, we can restrict ourselves to the scalar wave function of the field.

Let $E_1(x, y)$ be the wave function at the point z_1. Then the wave function $E(x, y)$ at the point z is

$$E(x,y) = \int dx_1 dy_1 P(x - x_1, y - y_1, z - z_1) E_1(x_1, y_1),$$
$$P(x,y,z) = \frac{1}{i\lambda z}\exp\left(i\pi\frac{x^2+y^2}{\lambda z}\right) \quad (1)$$

on the condition that there are no objects between points z_1 and z. Here, $P(x, y, z)$ is the Kirchhoff propagator in the paraxial approximation and λ is the radiation wavelength. If the longitudinal sizes of the objects do not differ significantly from the transverse sizes, we can neglect the changes in the trajectories of the rays during the passage through the objects, because the scattering angles are quite small (usually tens of microradians). In this case, when describing the interaction of radiation with an object, one can neglect the longitudinal length of the object and consider it flat and situated in the plane passing through the middle of its longitudinal extension. However, the object length is taken into account as an empty space. Sometimes this is important, e.g., for the composite refracting lens with a length comparable to its focal distance. Thus, the radiation–object interaction is described by multiplying the radiation field wave function by the so-called transmission function

$$T(x,y) = \exp\left(-i[\delta - i\beta]\frac{2\pi}{\lambda}t(x,y)\right), \quad (2)$$

where $t(x, y)$ is the local change in the material thickness inside the object along the z axis on the condition that the object consists of one material and δ and β are the quantities specifying the complex refractive index of the object material $n = 1 - \delta + i\beta$.

The calculation involves several steps and starts from the point source. Formally, the wave function in the plane of the source can be taken as the δ function, $E_0(x, y) = \delta(x, y)$. Substituting this expression into (1), we obtain the wave function in front of the object under study in the form of a Kirchhoff propagator. Next, it is necessary to multiply the wave function by the transmission function of the object, in which the specific form of the dependence $t(x)$ is taken into account, and apply (1) once again

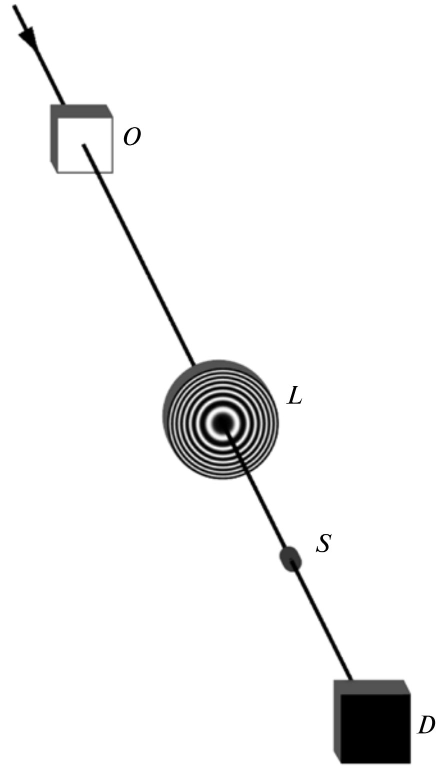

Fig. 1. Schematic of the Zernike phase contrast method for X rays. A nearly parallel synchrotron radiation beam is incident from the left and from above: (O) object, (L) refracting lens or zone plate, (S) phase-shifting plate, and (D) coordinate detector. In the case of imaging without enlargement, the object and detector are situated at the double focal length from the objective and the phase-shifting plate is at the point to which the source is focused.

$$E_2(x,y) = \int dx_1 dy_1 P(x - x_1, y - y_1, r_2 - r_1) \times T(x_1, y_1) E_1(x_1, y_1). \quad (3)$$

In the first calculation, r_2 is equal to the distance from the source to the focusing element (a refracting lens or a zone plate, Fig. 1). Then the calculation from formula (3) should be repeated with a new object in the form of the focusing element. In this case, the replacements $r_2 \to r_3$ and $r_1 \to r_2$ should be made. For a biconcave refracting parabolic lens, we have $t(x, y) = (x^2 + y^2)/R$, where R is the curvature radius at the parabola vertex. The infinite limits of integration are effectively cut off due to the absorption in the lens, since it is sufficiently thick at the aperture edges. For the zone plate, the absorption can be neglected and the problem of the integration limits remains. A zone plate has a finite aperture. Outside the aperture, the plate is uniform and has a thickness t_0. Inside the aperture of the zone plate, $t(x, y) = 0$ in the zones without material and $t(x, y) = t_0$ in the zones containing material. The zone boundaries are given by the formula $r_n = r_1(n)^{1/2}$,

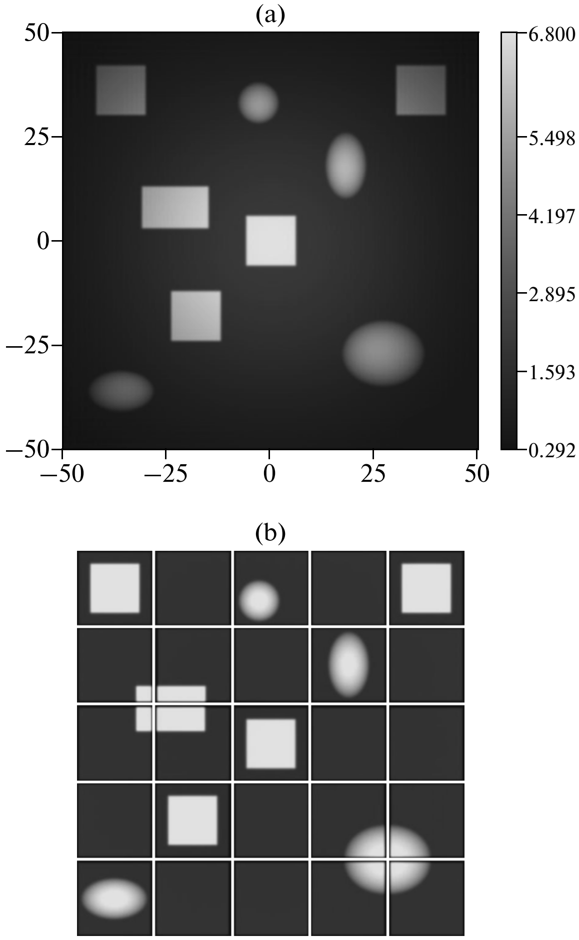

Fig. 2. Imaging of a series of silicon objects by a lens (a) without and (b) with the application of ptychography. The coordinate in micrometers is indicated by numbers.

where r_1 is the radius of the first zone and n is the zone number. In the third calculation, the object is a phase-shifting element with sizes of the same order of magnitude as the beam diameter in the objective focus. In this case, the replacements $r_2 \to r_4$ and $r_1 \to r_3$ should be made in (3).

Integral (3) is a convolution of two complex functions. It is convenient to calculate this integral with the use of a Fourier transform. First, the Fourier transform of the product of the functions of the arguments x_1 and y_1 was calculated. Then, it was multiplied by the Fourier transform of the Kirchhoff propagator, which has the analytical form $P(q_x, q_y, r) = \exp(-i\lambda r(q_x^2 + q_y^2)/4\pi)$. Finally, the inverse Fourier transform was calculated using the fast Fourier transform [9].

CALCULATION RESULTS FOR A SCHEME WITH A LENS

The calculations were performed for the standard parameters of the third-generation synchrotron sources. The distance from the source to the object $r_1 = 50$ m and the source size $S_0 = 50$ μm. A compound parabolic beryllium lens was considered the objective. The lens consisted of 60 elements with the radii of curvature $R = 50$ μm; the lens focal distance was 31.4 cm. The energy of the incident radiation was $E = 16$ keV. The calculation grid contained 1024 × 1024 points. Such a number of points resulted in a reasonable calculation time and caused no trouble with the array sizes. The source is incoherent in the sense that each of its points emits independently in phase. Since the source transverse dimension is S_0, the size of its image in the focus is $S = S_0(r_3 - r_2)/r_2$. The source sizes were taken into account by calculating the convolution of the intensity distribution for a point source and a Gaussian curve with a half-width $S_d = S_0(r_4 - r_2)/r_2$.

Figure 2a shows the image of a series of silicon objects of the same longitudinal size formed by the lens. We can see a gradual decrease in the intensity when moving from the center to the edge; the contrast also decreases in this case. The figure is cut at the edges, since artifacts appear near the boundaries of images. The main difficulty in performing two-dimensional calculations is that it is impossible to use a grid with a large number of points because a long computation time and a large memory are required. It is known that the FFT method has restrictions imposed on such parameters as the steps in the direct and reciprocal spaces and the size of the calculation domain in the direct space. These restrictions often give rise to artifacts in the object images. As a result, only the diffraction patterns from small objects with sizes much lower than that of the calculation domain are obtained sufficiently reliably. There are no such problems in the one-dimensional case, since large sizes of the calculation domain and small step can be set simultaneously.

It can be seen in Fig. 2a that the objects situated in the aperture center are imaged most clearly. However, the images of the same quality can be obtained for all the other objects using a method similar to ptychography. In this method, a large object is imaged not as a single whole but by parts. Each time the imaged part of the object is placed opposite of the region of the objective, an image of highest quality is yielded. For a lens, this region is the aperture center. Then, the images of the object portions are composed into a unified pattern. It is important that the imaged part of the object is separated by a slit, while the other part of the beam is blocked. Figure 2b shows the image of the same objects as in Fig. 2a, but obtained by the above-described method. In this case, the slit was placed in the aperture center and cut only the central region of the image, while the objects were moved with respect to the slit. It can be seen in Fig. 2b that such an approach allows a significant improvement of the image quality and leveling of the contrast.

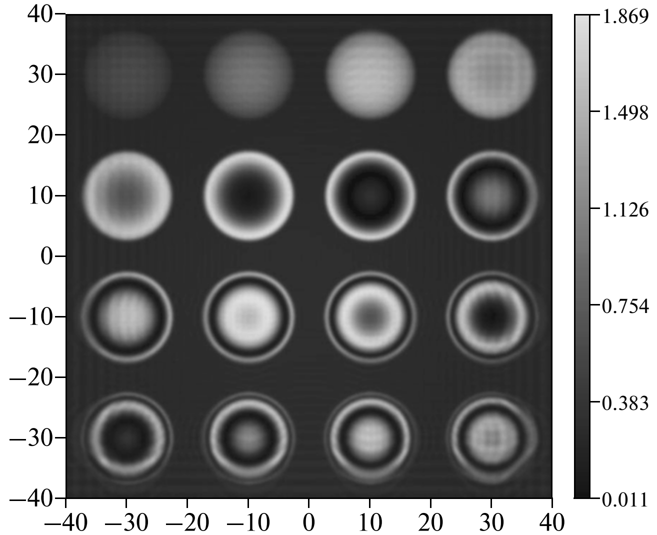

Fig. 3. Imaging of a series of ellipsoidal pores in a SiC crystal by a lens. The upper left pore has a longitudinal diameter of 3 μm and the next to the right is 5 μm in diameter; then, 5 μm is added to the diameter of each following pore.

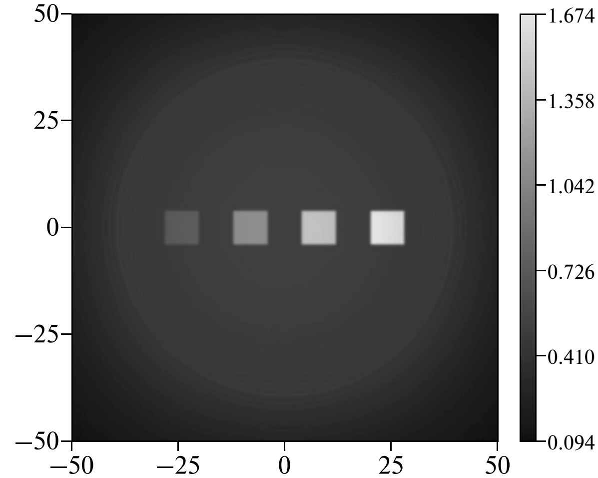

Fig. 4. Imaging of silicon rectangles of different longitudinal sizes by a lens with an aperture of 80 μm.

Using one-dimensional calculations, it was shown in [10] that specific oscillations appear in the image of elliptical objects elongated in the longitudinal direction. These oscillations allow one to determine the longitudinal size of the object. In this study, this result is confirmed by the two-dimensional calculations. Figure 3 shows the image of a series of ellipsoidal pores in the SiC crystal (the image is cut at the edges). In this case, like in [10], a dent in the substance rather than the phase-shifting plate was used. In Fig. 3, the upper left pore has a longitudinal diameter of 3 μm; the next to the right, is 5 μm in diameter. Then, 5 μm is added to the diameter of each following pore.

As the introduced phase shift increases, the intensity first increases. Then the intensity in the center decreases and characteristic oscillations appear in the center. The nature of the oscillations is as follows: the longitudinal thickness of the ellipsoidal pore decreases more and more rapidly as the distance increases from the center and so does the phase shift introduced by the pore. Each time when the phase shift 2π is "lost" in the pore, the pore transmission function is multiplied by the quantity $\exp(2\pi i) = 1$; i.e., it takes equal values. Thus, the oscillations, the thickness of which decreases with an increase in the distance from the center, appear in the pore image. With the total number of oscillations known, one can easily find out how many times the phase shift of 2π is accumulated in the pore and, thus, determine its longitudinal size.

Nevertheless, minor artifacts are seen at the edges of the images in Figs. 2 and 3. To obtain a nearly artifact-free image, a small-aperture lens should be considered as a focusing element. Figure 4 shows the imaging of silicon objects with a beryllium lens surrounded by an opaque slit with an aperture of 80 μm and a curvature radius R_0= 0.83 μm. The longitudinal size of the left-most object is 1 μm, which corresponds to the phase shift $\varphi \sim 0.2$; 1 μm is added to each next object. It can be seen that, like in the one-dimensional case, the height of the peak elevation is equal to the doubled phase shift introduced by the object.

CALCULATION RESULTS FOR A SCHEME WITH A ZONE PLATE

We considered a gold zone plate with an aperture A = 160 μm, a number of zones of 200, and a focal length F = 16 cm. In contrast to the refracting parabolic lens, the zone plate has many focusing orders. Even for the ideal zone plate, which shifts the wavefield phase by π in the zones, the first order, which accounts for 40% of the total intensity, is directly responsible for the image formation. The remaining 60% of the radiation are not directly involved in the image formation but interfere with the principal wave and, thus, decrease the image quality.

In this study we consider a perfect zone plane with no zero order. To eliminate the effect of the minus first order on the image formation, the object was placed not at the center but at some distance from the axis. In this case, the inverted image of the object in the first focusing order is formed in the opposite part of the zone plate aperture, while the unfocused image in the minus first order is produced in the same part of the aperture and outside of it; therefore, the two images do not overlap.

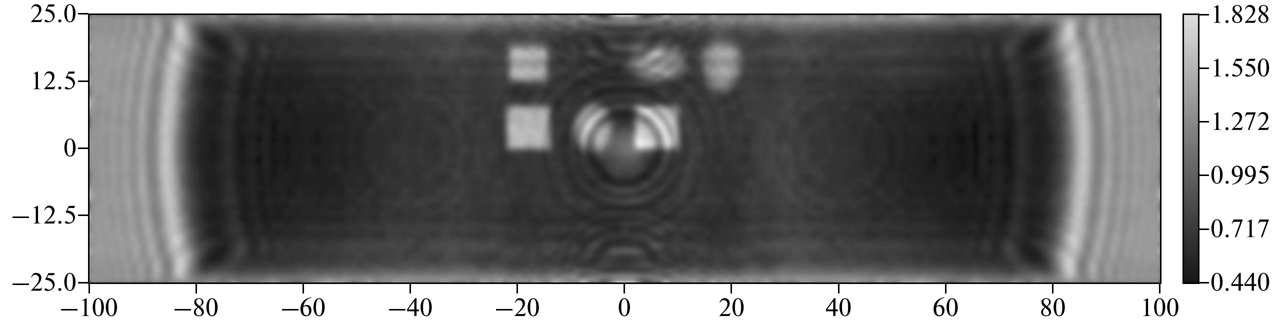

Fig. 5. Imaging of a series of silicon objects of the same longitudinal size by a zone plate.

Another reason for the image degradation is that the degree of coherence of the light beam is too high. Such a coherence level is known to frequently result in the formation of destructive speckles [11]. Therefore, a phase noise is intentionally produced in some experiments. In this study we averaged the calculated pattern with a Gaussian function of a certain half-width to suppress the parasitic interference of various orders. The optimal half-width was $S = 1.5$ μm.

Figure 5 shows the calculation results for the grid with 2048 × 512 points. The figure presents an image of a series of silicon objects of the same longitudinal size placed in the lower part of the central region of aperture. The image being inverted, the objects are seen in the upper half-plane. The image of the objects themselves is superimposed by the image of the central zones of the plate. It is also seen that the image of the central zone is repeated at the edges of the calculation domain. This is related to the fact that the Fourier integral is substituted by the Fourier series and to the existence of the minimum vector of the reciprocal lattice. The grid step in the q space is $dq = 2\pi/X$, where X is the size of the calculation domain. Since the number of grid points is even, there is no zero point and the minimum vector of the reciprocal lattice is $dq/2$. Therefore, the image in the direct space is periodic with a period of $X/2$. The intensity of these artifacts weakens with an increase in the distance from the center due to the presence of higher harmonics in the Fourier series.

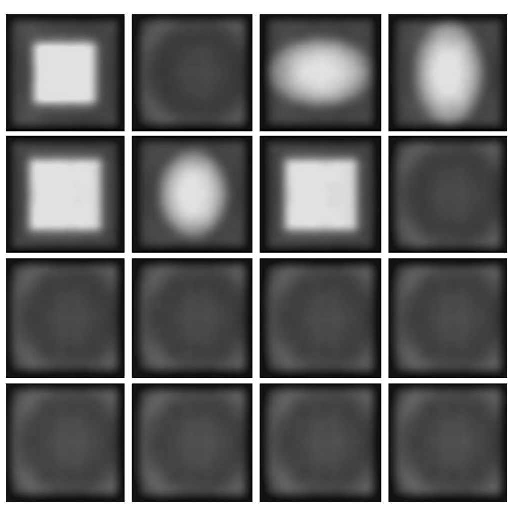

Fig. 6. The same as in Fig. 5 but with the application of ptychography.

As in the case of a lens, a method similar to ptychography can also be applied to imaging with a zone plate. However, in the latter case, the slit (diaphragm) cutting a part of the object should be placed not in the center but at a certain distance from it. In experiments, the object is placed closer to the aperture edge (where the zones are smaller) to increase resolution. In numerical simulation, the object should be situated so that, on the one hand, the zones are sufficiently small and, on the other hand, a sufficient number of points falling in one zone are provided to adequately describe the zone plate relief. Figure 6 shows images of the same objects as in Fig. 5, but obtained with the aid of ptychography. The slit center was at the point with the coordinates (0, −40). As for the case of a lens, this approach made it possible to improve the image.

CONCLUSIONS

The specific features of the Zernike phase contrast method in the two-dimensional case were studied by computer simulation. It was shown that the refracting lens as a focusing element allows better resolution than a zone plate. One specific feature of the two-dimensional calculations is that artifacts can appear in the images, especially in the scheme with a zone plate, because of the small number of points along both axes. The image can be corrected using ptychography. In the scheme with a lens, the slit should be placed in the aperture center; in the one with a zone plate, it should be closer to the aperture edge.

REFERENCES

1. A. Snigirev, I. Snigireva, V. Kohn, et al., Rev. Sci. Instrum. **66**, 5486 (1995).
2. V. G. Kohn, T. S. Argunova, and J. H. Je, Poverkhnost': Rentgen., Sinkhrotron. Neitron. Issled. **1**, 3 (2011).
3. F. Zernike, Z. Tekh. Fiz. **16**, 454 (1935).
4. G. Schmahl, D. Rudolph, P. Guttmann, et al., Rev. Sci. Instrum. **88**, 1282 (1995).
5. H. Yokosuka, N. Watanabe, T. Ohigashi, et al., J. Synchrotron Rad. **9**, 179 (2002).
6. Y. S. Chu, J. M. Yi, F. de Carlo, et al., Appl. Phys. Lett. **92**, 103119 (2008).
7. V. G. Kohn and M. A. Orlov, Poverkhnost': Rentgen., Sinkhrotron. Neitron. Issled. **11**, 76 (2010).
8. J. M. Rodenburg, Adv. Imag. Electron Phys. **150**, 87 (1996).
9. http://alglib.sources.ru/fft.
10. V. G. Kohn and M. A. Orlov, Crystallogr. Rep. **56** (6), 941 (2011).
11. D. L. White, O. R. Wood, and J. E. Bjorkholm, Rev. Sci. Instrum. **66**, 1930 (1995).

Translated by A. Zolot'ko